LAWRENCE
LIVERMORE
NATIONAL
LABORATORY

LLNL-JRNL-668979

Transparent Plastic Scintillators for Neutron Detection Based on Lithium Salicylate

A. N. Mabe

March 24, 2015

Nuclear Instruments and Methods in Physics Research Section A

Disclaimer

Transparent Plastic Scintillators for Neutron Detection Based on Lithium Salicylate

Andrew N. Mabe*, Andrew M. Glenn, M. Leslie Carman, Natalia P. Zaitseva, Stephen A. Payne

Lawrence Livermore National Laboratory
7000 East Avenue
Livermore, CA 94551, USA

Abstract: Transparent plastic scintillators with pulse shape discrimination containing lithium-6 salicylate have been synthesized by bulk polymerization with a maximum lithium-6 loading of 0.40 wt%. Photoluminescence and scintillation responses to gamma-rays and neutrons are reported herein. Plastics containing lithium-6 salicylate exhibit higher light yields and permit a higher loading of lithium-6 as compared to previously reported plastics based on lithium 3-phenylsalicylate. However, pulse shape discrimination performance is reduced in lithium salicylate plastics due to the requirement of adding more nonaromatic monomers to the polymer matrix as compared to those based on lithium 3-phenylsalicylate. Reduction in light yield and pulse shape discrimination performance in lithium-loaded plastics as compared to pulse shape discrimination plastics without lithium is interpreted in terms of energy transfer interference by the aromatic lithium salts.

Keywords – Neutron detector, plastic scintillator, lithium salicylate, pulse shape discrimination

*Corresponding Author
Lawrence Livermore National Laboratory
7000 East Avenue
Livermore, CA 94551, USA
1 (925) 423-9308
mabe2@llnl.gov

LLNL-JRNL-668979

1. Introduction

Neutron detection is relevant to the fields of nuclear physics, nuclear power generation, homeland security, oil well logging, and medical imaging [1, 2]. Gas tubes filled with helium-3 are widely used to detect neutrons in the presence of gamma-ray background but due to the shortage of this material, many efforts have been made to develop replacement technologies for neutron detection. Among these technologies, plastic scintillators are relevant candidates due to their low cost, fast decay times, wide range of environmental stability, low toxicity, ease of handling, and ease of scaling to large volumes. Fast neutrons produce signals in plastic scintillators by elastic scattering from hydrogen atoms which generate recoil protons with kinetic energy sufficient to ionize and excite the surrounding matrix. These ionizations and excitations produce a flash of light which is detectable by a photomultiplier tube (PMT). Unambiguous detection of the presence of neutrons is often complicated by gamma-ray background which produces Compton-scattered electrons in the scintillator. These Compton-scattered electrons generate signals inside the scintillator which overlap with signals generated by neutrons.

One method by which scintillators can be used to discriminate between neutrons and gamma-rays exploits the difference in the time required for light to be emitted in response to energy deposition by the different radiation quanta. Compton-scattered electrons deposit energy over a large area, usually on the order of millimeters, whereas heavy ions such as recoil protons generated by fast neutrons deposit energy over a very short distance, usually on the order of micrometers. The higher concentration of ionizations and excitations leads to an enhanced probability of triplet-triplet annihilation which results in delayed fluorescence. Thus, heavy ions produce signals over a longer timescale than gamma-rays. This time difference in signal generation can be exploited to determine if the energy was deposited by a heavy ion or a gamma-ray and is known as pulse shape discrimination (PSD). The first PSD plastic was reported by Brooks et. al. in 1960 which comprised *p*-terphenyl and isopropylbiphenyl in a polyvinyltoluene matrix [3]. This plastic formulation, which comprises *p*-terphenyl and isopropylbiphenyl in a polyvinyltoluene matrix, is unstable after a short period of time and results in an unusable opaque material [4]. Recently, plastic scintillators with PSD and improved stability have been developed using different strategies [5-7]. Since the development of these materials, improvements, variations, and characterizations by multiple groups have been made [4, 8-12]. These materials are summarized well in a recent review article [13].

Moderation around neutron-emitting materials can partially thermalize the resulting neutron energy spectrum. These thermalized neutrons can be detected by capture reactions that result in the emission of ionizing radiation that has sufficient kinetic energy to induce signals inside a detector. Common nuclides used for this purpose include ^{6}Li, ^{10}B, and ^{157}Gd. Addition of these nuclides adds new functionality to PSD plastics in that they become capable of generating usable signals from both fast and thermal neutrons [14, 15]. After neutron capture, ^{157}Gd emits gamma-rays over a range of energies so it is not an ideal neutron capture element for PSD plastics. As was known before PSD plastics were developed, carborane can be loaded into plastics to produce transparent scintillators capable of detecting thermal neutrons via the ^{10}B capture reaction [16]. Pawełczak et. al. demonstrated that this can be applied to PSD plastics to produce optically transparent scintillators which are capable detecting thermal neutrons by the ^{10}B capture reaction as well as fast neutrons [14]. Zaitseva et. al. demonstrated that lithium 3-phenylsalicylate (LiPSA) can be loaded into PSD plastics to produce transparent scintillators which are capable of detecting thermal neutrons via the ^{6}Li capture reaction as well as fast neutrons [15]. Lithium-loading in PSD plastics was also accomplished utilizing lithium pivalate by Cherepy et. al. [17]. Even though the thermal neutron capture cross section of ^{6}Li is lower than that of ^{10}B (942 vs 3840 barns, respectively [2]), ^{6}Li may have advantages as compared to ^{10}B in PSD plastics.

Thermal neutron capture by ^{6}Li produces an alpha particle and a triton with a reaction energy of 4.78 MeV. Thermal neutron capture by ^{10}B results in two possible reactions: release of an alpha particle and a ^{7}Li nucleus with a reaction energy of 2.79 MeV (6%) and release of an alpha particle and ^{7}Li nucleus with 2.31 MeV as well as a 0.48 MeV gamma-ray (94%). The gamma-ray is undesirable in PSD plastics because it results in a faster average scintillation time corresponding to the neutron capture reaction.

The incorporation of ^{6}Li by dissolution in pure aromatic plastics has proven to be difficult and currently only a few compositions exist. Martinez et. al. recently demonstrated that copolymerizing aromatic and nonaromatic monomers such as styrene and methyl methacrylate produces PSD-capable plastics with improved mechanical properties. Although incorporation of nonaromatic monomers reduces the scintillation performance as compared to pure aromatic matrices [9], it opens up the realm of possibilities of incorporating ^{6}Li-bearing compounds which are soluble in nonaromatic matrices such as poly(methyl methacrylate) (PMMA) but insoluble in aromatic matrices such as polystyrene (PS) into PSD-capable plastics. The present work seeks to expand the development of PSD plastics which can detect thermal neutrons. In particular, we found that suitable processing procedures permit the incorporation of lithium-6 salicylate ($^{6}LiSal$), which is cheaper and easier to purify than $^{6}LiPSA$, into PSD plastics. An image comparing the molecular structures of LiSal and LiPSA is shown in Fig. 1. While the implementation of $^{6}LiSal$ as component of a scintillation detector is not a new concept [18-21], the work presented herein represents the first report of which the authors are aware of $^{6}LiSal$ existing as a dissolved component inside a transparent plastic scintillation detector.

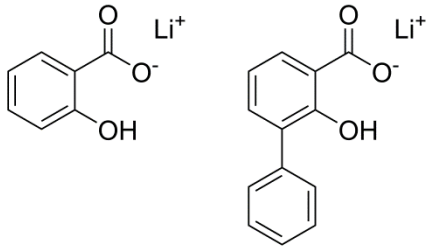

Fig. 1. Molecular structures of LiSal and LiPSA.

2. Materials and Methods

All chemicals were obtained from Sigma-Aldrich unless otherwise stated. Toluene, acetone, diethyl ether, methanol, tetrahydrofuran (THF), dimethoxyethane (DME) salicylic acid (Fluka), scintillation grade 2,5-diphenyloxazole (PPO), and scintillation grade 1,4-bis(2-methylstyryl)benzene (bis-MSB) were used as received. Styrene, methyl methacrylate (MMA), divinylbenzene (DVB), and ethylene glycol dimethacrylate (EGDMA) were passed through a column containing basic alumina on top of silica to remove inhibitors and impurities, then were sparged for 45 minutes with a steady stream of dry nitrogen and stored in an inert atmospherer at -20°C until needed. Free radical initiator 1,1-di(*t*-butylperoxy)-3,3,5-trimethylcyclohexane (L-231, obtained from Luperox®) was sparged for 45 minutes with a steady stream of dry nitrogen and kept at -20°C until needed. ^{6}Li metal (95% ^{6}Li) suspended in mineral oil was washed with toluene and acetone before use. Water was passed through Milli-Q water purification system before use. PSA (TCI America) was recrystallized six times from a 10:1 toluene:acetone solution and collected by vacuum filtration.

Anhydrous $^{6}LiOH$ was synthesized by reacting small pieces of washed ^{6}Li metal in a 1:1 solution of methanol and water, then evaporating the solvents. The material was suspended in diethyl ether, filtered, and washed with diethyl ether and acetone to remove any residual mineral oil. The resulting

$^{6}LiOH \cdot H_2O$ was dissolved in methanol which was then evaporated under vacuum at 150°C for four hours to give anhydrous $^{6}LiOH$. $^{6}LiSal$ was synthesized by titrating salicylic acid with $^{6}LiOH$ in methanol to pH = 6. The solvent was evaporated and the resulting crude material was washed with anhydrous diethyl ether to remove excess salicylic acid. The resulting purified material was dried on a Schlenk line at 90°C under nitrogen for four hours to remove residual solvents. $^{6}LiPSA$ was synthesized by titrating purified PSA with $^{6}LiOH$ in methanol, evaporating the solvent, washing with diethyl ether, and drying on a Schlenk line at 90°C under nitrogen for four hours to remove residual solvents. Vials used for polymerization were cleaned with acetone and dried in an oven at 110°C, then further dried with a torch immediately before use.

Plastic scintillators based on $^{6}LiPSA$ were fabricated according to previously reported procedures [15]. Plastic scintillators based on $^{6}LiSal$ were made by dissolving $^{6}LiSal$ in THF in a flame-dried scintillation vial, then evaporating the solvent under a stream of dry nitrogen until a constant mass was obtained. PPO and bis-MSB were added to the vial which was then capped, degassed, then placed into a glovebox. The vial was charged with appropriate masses of styrene, MMA, crosslinker, and L-231 in the glovebox, sealed with vinyl tape, and removed from the glovebox. For plastics in which more than half the matrix was styrene, 5% DVB was added and for plastics in which more than half the matrix was methyl methacrylate, 1% EGDMA was added. Small plastics were fabricated with a total mass of 10 g and large plastics were fabricated with a mass of 89 g before machining. Polymerization was conducted by placing the charged vial in a nitrogen-purged oven. For Ø24 mm plastics, the polymerization program was 60°C for 1 day, 65°C for 1 day, then 70°C for 4 days. For larger diameter plastics, the temperature program was 59°C for 3 days, 65°C for 1 day, and 70°C for 6 days. After polymerization, the vials were removed from the oven, cooled to room temperature, and the plastic cylinders were retrieved by breaking the vials. The faces of the plastic cylinders were machined and polished before characterization

Fluorescence measurements were conducted using a Horiba Jobin Yvon Fluoromax-4 spectrometer equipped with a 450 W Xe lamp in reflectance mode in which the front face of the scintillator was irradiated by the incident photons and the emission from that same face was recorded. Fluorescence spectra were corrected for the wavelength-dependent intensity of the lamp and spectral sensitivity of the detector PMT. Scintillation responses were characterized by wrapping the polished plastics with Teflon tape leaving an exposed face which was coupled with optical grease to a Hamamatsu R6231-100-SEL PMT. Signals collected from the PMT were recorded using a 14-bit high resolution CompuScope 14200 waveform digitizer at a sampling rate of 200 MS/s. Light yields were evaluated from the ^{137}Cs gamma-ray response for which the 500 keVee location was defined by the 50% position of the Compton edge. The plastics were exposed to a ^{252}Cf source moderated by 5.1 cm of lead and high density polyethylene. Three inches of polyethylene was used for Ø24 mm plastics and four inches was used for larger plastics. Resulting waveforms were integrated over two time integrals, t_{total} and t_{tail}, corresponding to the total charge (Q_{total}) and the delayed component of the signal (Q_{tail}), respectively. The ratio $R = Q_{tail}/Q_{total}$ indicated whether an event was likely produced by a neutron (large R) or a gamma-ray (small R). Quantification of the PSD was accomplished by calculating standard figures of merit (FoM) as defined in Eq. 1

$$FoM = \frac{\langle n \rangle - \langle \gamma \rangle}{FWHM_n + FWHM_\gamma} \quad (1)$$

where $\langle n \rangle$ is the centroid of the thermal or fast neutron distribution, $\langle \gamma \rangle$ is the centroid of the gamma-ray distribution, and $FWHM_n$ and $FWHM_\gamma$ are the full widths at half maximum of the fast or thermal neutron and gamma-ray distributions, respectively. The time gates were optimized to maximize the FoM

as previously described [15]. As an example, for a lithium-loaded plastic the optimization resulted in classifying the first 45 ns after the peak as the prompt component and out to 1125 ns as the delayed component. FoM were calculated separately for thermal neutron/gamma-ray discrimination and fast neutron/gamma-ray discrimination. Thermal neutron/gamma-ray FoM was calculated by fitting the thermal neutron distribution to a Gaussian function and running the calculation over the energy region ±2.5σ around the centroid of the thermal neutron distribution. Fast neutron/gamma-ray discrimination was calculated over the energy range 450 – 510 keVee unless otherwise noted. The error in the figure of merit calculations is expected to be around 3%. It was difficult to calculate a reliable and reproducible FoM for thermal neutron/fast neutron discrimination due to the high degree of overlap between these two sets of signals so discrimination between fast and thermal neutrons will not be discussed in this work.

3. Results and Discussion

3.1. Optical Transparency

Compositions in terms of percentage of the total mass of the fabricated plastics are shown in Table 1. The remainder of the mass comprises the matrix, crosslinker at concentrations described in section 2, and any chelating solvent. The weight percentages of lithium are calculated based on the amounts of corresponding salts added to the initial mixture. It was previously reported that plastics containing 0.2% ^{6}Li at appropriate thicknesses can have thermal neutron detection efficiencies as high as 50% [15], so plastics in this work were fabricated around this concentration. Light yields given as relative values to pure polystyrene (PS) plastics containing PS containing 30% PPO and 0.2% bis-MSB. Plastics containing 2.8, 5, and 9.5 wt% ^{6}LiSal with varying ratios of PS and PMMA were fabricated to investigate the effect of changing the aromatic fraction of the matrix and increasing the concentration of the salt on the scintillation performance. Plastics containing 5% ^{6}LiSal were transparent at a matrix containing up to 30% PS and plastics containing 9.5% ^{6}LiSal were only transparent up to 5% PS. Plastics containing ^{6}LiPSA at up to 7.6% were transparent in a matrix containing 85% PS. Matrix compositions were prepared with varying ratios of PS to PMMA to compare the effects of increasing the salt concentration and matrix composition on scintillation performance. Plastics containing more than 0.40% ^{6}Li as ^{6}LiSal and more than 0.21% ^{6}Li as ^{6}LiPSA were not transparent. Samples containing ^{6}LiSal and ^{6}LiPSA at 0.12% ^{6}Li with optimized matrix compositions for each were fabricated at Ø51 × 24.5 mm to illustrate the potential for scaling these plastics to larger sizes. An image of the Ø51 mm plastics is shown in Fig. 2.

Table 1. Compositions by Mass of Fabricated Plastics

Sample	*Matrix*	*PPO*	*bis-MSB*	*Li*	*wt% ^{6}Li*	*Dimensions*
1	PS	30%	0.2%	None	0%	Ø24 × 16.5 mm
2	PMMA	30%	0.2%	None	0%	Ø24 × 16.5 mm
3	85PS:15PMMA	30%	0.2%	None	0%	Ø24 × 16.5 mm
4	PMMA	30%	0.2%	5% ^{6}LiSal	0.21%	Ø24 × 16.5 mm
5	5PS:95PMMA	30%	0.2%	5% ^{6}LiSal	0.21%	Ø24 × 16.5 mm
6	10PS:90PMMA	30%	0.2%	5% ^{6}LiSal	0.21%	Ø24 × 16.5 mm
7	15PS:85PMMA	30%	0.2%	5% ^{6}LiSal	0.21%	Ø24 × 16.5 mm
8	20PS:80PMMA	30%	0.2%	5% ^{6}LiSal	0.21%	Ø24 × 16.5 mm
9	25PS:75PMMA	30%	0.2%	5% ^{6}LiSal	0.21%	Ø24 × 16.5 mm
10	30PS:70PMMA	30%	0.2%	5% ^{6}LiSal	0.21%	Ø24 × 16.5 mm

11	30PS:70PMMA	30%	0.2%	7.6% ^{6}LiPSA	0.21%	Ø24 × 16.5 mm
12	PMMA	30%	0.2%	9.3% ^{6}LiSal	0.39%	Ø24 × 16.5 mm
13	5PS:95PMMA	30%	0.2%	9.5% ^{6}LiSal	0.40%	Ø24 × 16.5 mm
14	30PS:70PMMA	30%	0.2%	2.8% ^{6}LiSal	0.12%	Ø24 × 16.5 mm
15	85PS:15PMMA	30%	0.2%	4.3% ^{6}LiPSA	0.12%	Ø24 × 16.5 mm
16	30PS:70PMMA	30%	0.2%	2.8% ^{6}LiSal	0.12%	Ø51 × 24.5 mm
17	85PS:15PMMA	30%	0.2%	4.3% ^{6}LiPSA	0.12%	Ø51 × 24.5 mm

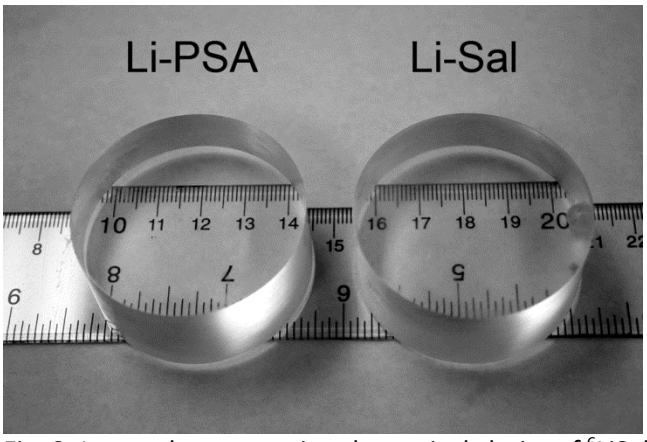

Fig. 2. Image demonstrating the optical clarity of ^{6}LiSal and ^{6}LiPSA plastics with dimensions Ø51 × 24.5 mm.

Pure ^{6}LiSal is insoluble in both styrene and methyl methacrylate monomers which precludes the possibility of synthesizing a transparent styrene- or methyl methacrylate-based plastic containing ^{6}LiSal by bulk polymerization using only those components. However, the initial dissolution of ^{6}LiSal in THF permits subsequent dissolution in liquid monomers and increases the solubility of the salt in plastics up to 9.5 wt%. After evaporating the THF from ^{6}LiSal, a 1:2 mole ratio of ^{6}LiSal:THF remained which was soluble in methyl methacrylate and did not become turbid on addition of styrene monomer. A possible explanation which accounts for this phenomenon is that the ^{6}LiSal forms an adduct with two THF molecules as shown in Fig. 3 in which the hard donor oxygen atoms on the THF molecules donate electron density to the lithium ion. This result is in agreement with accepted complexation chemistry in that lithium ions commonly form complexes with anions and donor ligands as 4-coordinate complexes which are the most favorable conformation from an electrostatic point of view [22]. This tetracoordinated geometry reduces the effective charge on the lithium ion and shields the ionic charge from surrounding weakly polar monomers, thereby facilitating solubility in the resulting polymerized matrix. This explanation is further supported by the observation that the masses of the machined plastics have remained stable for six months, indicating that the THF is likely stable inside the plastics. Likewise, ^{6}LiPSA is also insoluble in liquid styrene and methyl methacrylate monomers. By first dissolving it in liquid PPO at an elevated temperature or DME, solubility of ^{6}LiPSA in liquid monomers and resulting polymerized matrices is improved. It is suspected that ^{6}LiPSA forms an adduct with the nitrogen or oxygen atoms of the PPO molecule or the oxygen atoms of DME which, like ^{6}LiSal complexed with THF, results in enhanced solubility in plastics due in part to shielding the charge on the ions from the surrounding matrix. This framework partially explains the current observations but unfortunately still does not provide a method by which transparent lithium-loaded plastic formulations can be predicted.

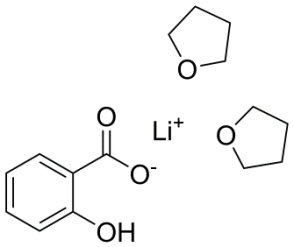

Fig. 3. Suggested structure of the ^{6}LiSal:2THF adduct.

3.2. Fluorescence Spectra

Emission spectra from plastics containing no lithium, ^{6}LiSal, and ^{6}LiPSA are shown in Fig. 4. The results indicate that the primary emission shape is that of the secondary dye (bis-MSB), but the spectra of the plastics containing lithium are slightly distorted. Most noticeably, the recorded emission from PPO in the region around 368 nm is markedly reduced in the plastics containing lithium as compared to the plastic without lithium. This suggests that some of the excitons on PPO are transferred to the lithium salts. Because the lithium compounds are aromatic, it is expected that they participate in the photon cascade in which some of the excitons are transferred from the matrix and from PPO to the lithium salts rather than to bis-MSB, thereby resulting in a noticeable difference in the overall emission spectra.

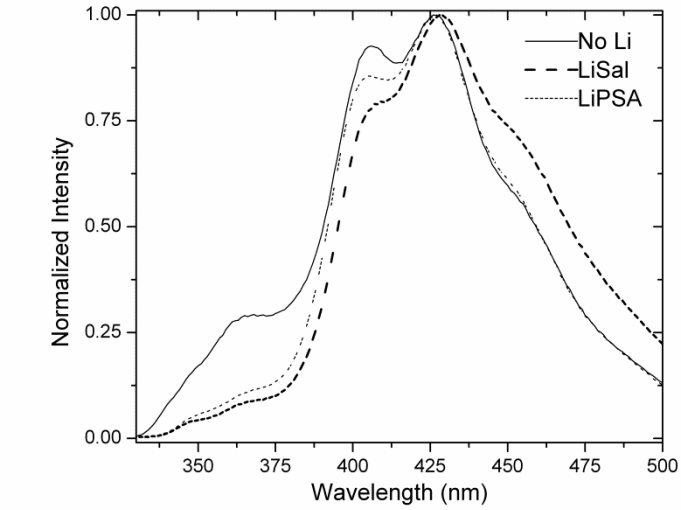

Fig. 4. Emission spectra of plastics containing no lithium, ^{6}LiSal, and ^{6}LiPSA. Spectra were obtained in reflectance mode by exciting the styrene subunits at 275 nm and recording the resulting emission.

The data in Fig. 5 illustrate normalized PS emission, PPO emission, LiSal excitation, and LiPSA excitation spectra. The excitation spectra of LiSal and LiPSA were measured using PMMA plastics containing 0.12% ^{6}Li to in order to obtain molecular excitation in the solid state while avoiding any matrix effects due to PS absorption. The overlap of LiPSA excitation with PPO emission is greater than that for LiSal, indicating that the energy transfer from PPO to LiPSA is more efficient than from PPO to LiSal. Due to the lower scintillation efficiencies of pure LiSal and LiPSA as compared to the more efficient secondary dyes used for the preparation of PSD plastics, a greater degree of energy transfer to the lithium salts rather than to bis-MSB should result in a decrease in scintillation efficiency for the plastics described herein.

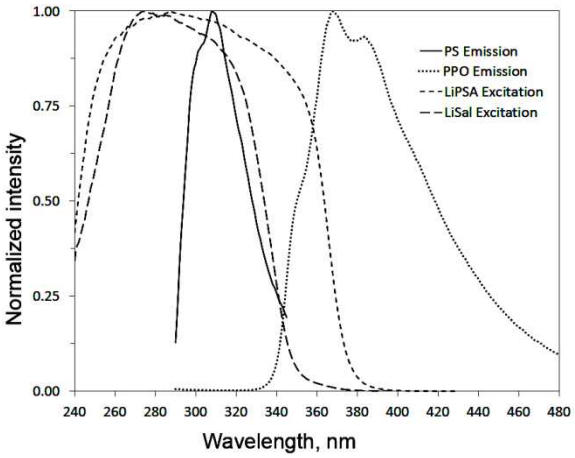

Fig. 5. PS emission, PPO emission, LiSal excitation, and LiPSA excitation. Spectra are normalized to the maximum intensity value of each response.

3.3. Effects on Scintillation Performance

Plots demonstrating PSD in Ø51 × 24.5 mm plastics containing ^{6}LiSal and ^{6}LiPSA at 0.12% ^{6}Li exposed to ^{252}Cf are shown in Fig. 6. The left column illustrates the responses from the ^{6}LiSal plastic and the right column illustrates those from the ^{6}LiPSA plastic. The top row contains plots illustrating PSD between fast neutrons and gamma-rays in the energy region around the ^{137}Cs. FoM calculations were made using Eq. 1. The center row illustrates the total response from ^{252}Cf plotted as Q_{tail}/Q_{total} versus energy in keV_{ee}. The bottom row illustrates the PSD between thermal neutrons and gamma-rays in the region around the thermal neutron capture spot. As shown in Fig. 6, both plastics exhibit separation between fast neutrons and gamma-rays above about 80 keV_{ee} as well as the presence of a spot corresponding to the thermal neutron capture reaction by ^{6}Li. Similar evaluations were made for all fabricated plastics and the results are shown in Table 2 for which FoM ($n_{th,\gamma}$) is the figure of merit for thermal neutrons and gamma-rays and FoM ($n_{f,\gamma}$) is the figure of merit for fast neutrons and gamma-rays. All plastics shown are Ø24 × 16.5 mm except plastics 16 and 17 which are Ø51 × 24.5 mm. The light yields are normalized to that of the plastic comprising PS, 30% PPO, and 0.2% bis-MSB. The presence of PMMA in the plastics decreases the light yield and PSD performance with the deleterious effects being proportional to concentration of PMMA. This is most clearly seen by comparing plastics 1 and 3 which do not contain ^{6}Li for which both the light yields and the FOMs drops significantly on going from a pure PS matrix to a pure PMMA matrix. This effect is also evident among the plastics containing 5% ^{6}LiSal for which the light yields decrease consistently with increasing fraction of PMMA in the matrix. This result is reasonable by considering that the energy deposited on a methyl methacrylate unit is not transferred to a fluorescent entity whereas if the energy is deposited on a styrene unit, a fraction of the energy is transferred to the fluors. Thus, decreasing the fraction of styrene units in the matrix relative to methyl methacrylate units decreases the number of excitons available to be transferred to the fluors, thereby resulting in fewer emitted optical photons per scintillation event.

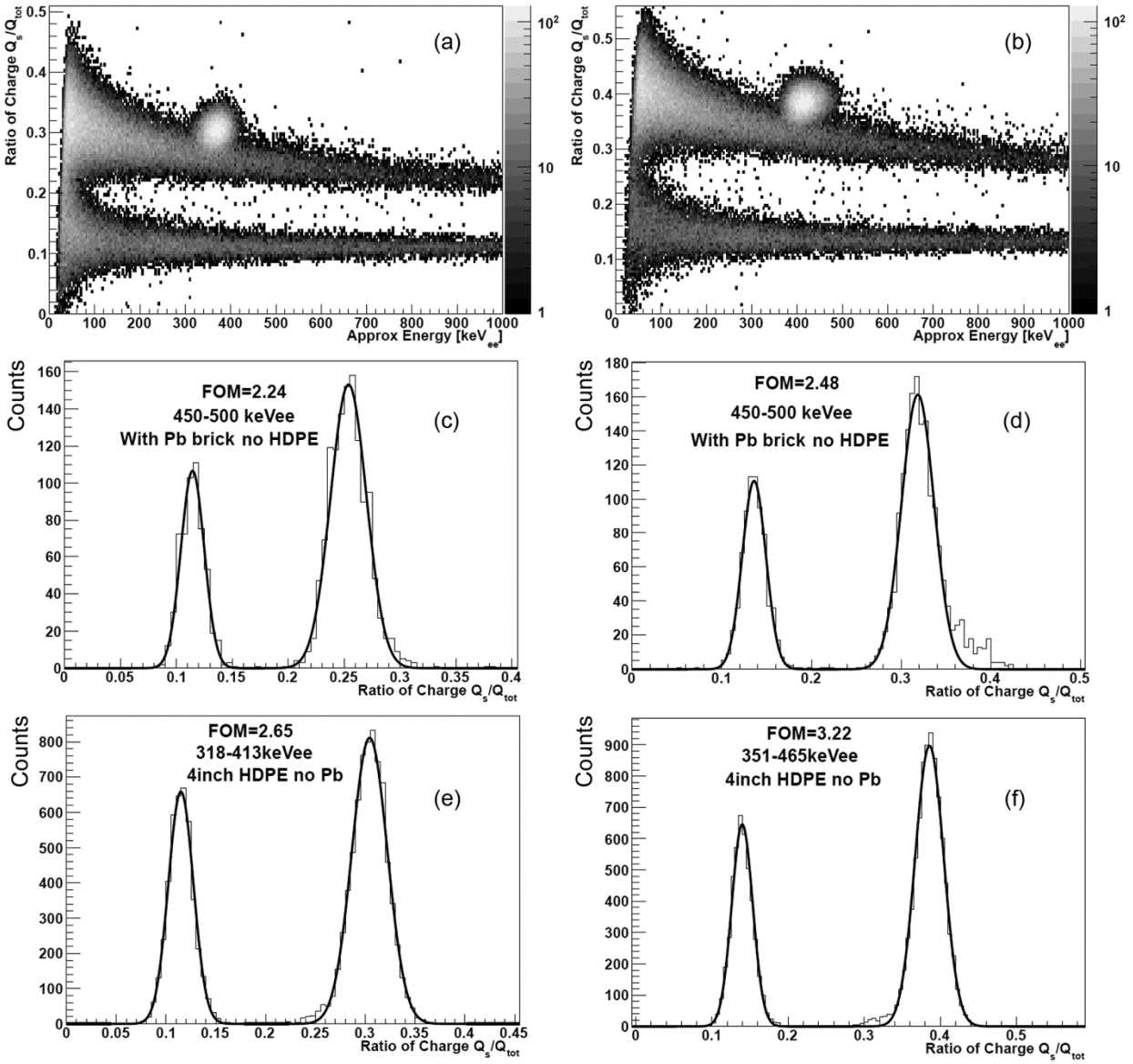

Fig. 6. Plots illustrating PSD in Ø51 × 24.5 mm plastics containing ^{6}LiSal (left column) and ^{6}LiPSA (right column). (a) and (b): Scatter plots illustrating the total responses from ^{252}Cf; (c) and (d): PSD between fast neutrons and gamma-rays in the energy region around the Compton edge; (e) and (f): PSD between thermal neutrons and gamma-rays in the energy region around the thermal neutron capture spot.

Table 2. Scintillation Responses of Fabricated Plastics

Sample	*Matrix*	*Li*	*Light Yield (A.U.)*	*FoM ($n_{th,\gamma}$)*	*FoM ($n_{f,\gamma}$)*
1	PS	None	1.00 ± 0.05	N/A	3.03
2	PMMA	None	0.74 ± 0.04	N/A	2.58
3	85PS:15PMMA	None	0.98 ± 0.05	N/A	3.06
4	PMMA	5% ^{6}LiSal	0.57 ± 0.03	2.43	2.15
5	5PS:95PMMA	5% ^{6}LiSal	0.59 ± 0.03	2.59	2.36
6	10PS:90PMMA	5% ^{6}LiSal	0.59 ± 0.03	2.64	2.14

7	15PS:85PMMA	5% ^{6}LiSal	0.59 ± 0.03	2.65	2.30
8	20PS:80PMMA	5% ^{6}LiSal	0.59 ± 0.03	2.70	2.51
9	25PS:75PMMA	5% ^{6}LiSal	0.65 ± 0.03	2.97	2.33
10	30PS:70PMMA	5% ^{6}LiSal	0.70 ± 0.04	2.99	2.49
11	30PS:70PMMA	7.6% ^{6}LiPSA	0.57 ± 0.03	2.86	2.44
12	PMMA	9.3% ^{6}LiSal	0.55 ± 0.03	2.33	2.00
13	5PS:95PMMA	9.5% ^{6}LiSal	0.62 ± 0.03	2.67	2.32
14	30PS:70PMMA	2.8% ^{6}LiSal	0.63 ± 0.03	2.72	2.21
15	85PS:15PMMA	4.3% ^{6}LiPSA	0.56 ± 0.03	3.30	2.33
16	30PS:70PMMA	2.8% ^{6}LiSal (Ø51 × 24.5 mm)	0.58 ± 0.03	2.65	2.24
17	85PS:15PMMA	4.3% ^{6}LiPSA (Ø51 × 24.5 mm)	0.52 ± 0.03	3.22	2.48

As shown in the results, the presence of aromatic ^{6}Li salts in the plastics decreases the light yield and PSD performance relative to the plastics without ^{6}Li salts. This implies that the lithium salts are acting as exciton traps which only weakly scintillate. This means that a large fraction of the excitons that are transferred to or absorbed by the salts rather than to the fluors are lost vibrationally rather than resulting in emission of an optical photons. Thus, the presence of the aromatic lithium salts is expected to decrease the observed light yield. It is also observed that the FoM between fast neutrons and gamma rays is reduced on addition of the aromatic lithium salts. This is likely due to triplet harvesting by the lithium salts. Triplet traps such as the aromatic lithium salts decrease the average lifetime of the triplet states in the scintillator, thereby decreasing the concentration and therefore the rate of delayed emission and resulting in a faster average delayed component of the resulting waveforms from fast neutrons. This implies that the use of lithium salts which have absorption bands below that of styrene and PPO would not interfere with the energy transfer processes in plastics, thereby preventing decreases in light yield and PSD due to exciton trapping.

Comparing plastics 10 and 11 which contain ^{6}LiSal and ^{6}LiPSA, respectively, at 0.21% ^{6}Li indicates that the light yield of the ^{6}LiPSA plastic is lower than that of the ^{6}LiSal plastic. Due to the similarity in the atom types in ^{6}LiSal and ^{6}LiPSA, it cannot be concluded that the initial number or density of ionizations and excitations is very different between the ^{6}LiSal and ^{6}LiPSA plastics. The data in Fig. 5 show that the transfer of singlet excitation energy is more efficient from PS and PPO to ^{6}LiPSA as compared to ^{6}LiSal. This makes it reasonable to conclude that after the energy is deposited in the scintillator, ^{6}LiPSA collects more of the energy from PPO than ^{6}LiSal does; thus, more of the energy is lost to vibrational de-excitation rather than being converted into light detectable by the PMT. The difference in PSD between plastics 9 and 10 is likely not outside the error of the measurement. This is an interesting result because pure LiPSA crystals show significantly better PSD than pure LiSal crystals [15, 21]. This suggests that at the concentrations explored in this work, the PSD properties of the ^{6}Li-bearing salt do not influence the PSD properties of the overall plastic. However, by comparing plastics 14 with 15 as well as plastics 16 with 17, it can be seen that better PSD can be achieved with ^{6}LiPSA plastics as compared to ^{6}LiSal plastics due to higher solubility of ^{6}LiPSA in matrices with a greater aromatic fraction.

4. Conclusions

This work has demonstrated that ^{6}LiSal can be incorporated into PSD plastics to produce transparent scintillation detectors at up to 0.40 wt% ^{6}Li. Though the current scintillation performance of lithium-loaded plastic scintillators is still inferior to that of unloaded plastic scintillators, improvements have been made in the neutron detection efficiency, light yield, cost, and ease of production of lithium-loaded PSD plastics with ^{6}LiSal as compared to with ^{6}LiPSA. This work also extended the possibility of using low-cost and easy to purify materials to produce lithium-loaded PSD plastics easily and showed that the complexation strategy implemented for ^{6}LiPSA to produce transparent lithium-loaded plastic scintillators is not an isolated case. Both ^{6}LiSal and ^{6}LiPSA interfere with the photon cascade with a concomitant decrease in light yield and PSD performance relative to the unloaded plastics. Both ^{6}Li salts collect excitation energy from PS and PPO but the effect is more pronounced with ^{6}LiPSA, thereby resulting in lower light yields as compared to ^{6}LiSal for similar matrices. However, for comparable matrices there was no significant difference in PSD performance between the two salts.

Acknowledgments

This work was performed under the auspices of the U.S. DOE by Lawrence Livermore National Laboratory under Contract DE-AC52-07NA27344. Financial support was provided by the U.S. Department of Energy Office of Nonproliferation Research and Development (NA-22).

References

[1] J.B. Birks, The theory and practice of scintillation counting, Pergamon Press, New York, 1964.
[2] G.F. Knoll, Radiation detection and measurement, 4th ed., John Wiley & Sons, Inc., New York, 2010.
[3] F.D. Brooks, R.W. Pringle, B.L. Funt, Pulse shape discrimination in a plastic scintillator, IRE Trans. Nucl. Sci., 7 (1960) 35-38.
[4] P. Blanc, M. Hamel, C. Dehé-Pittance, L. Rocha, R.B. Pansu, S. Normand, Neutron/gamma pulse shape discrimination in plastic scintillators: Preparation and characterization of various compositions, Nucl. Instrum. Meth. A, 750 (2014) 1-11.
[5] N. Zaitseva, B.L. Rupert, I. Pawełczak, A. Glenn, H.P. Martinez, L. Carman, M. Faust, N. Cherepy, S. Payne, Plastic scintillators with efficient neutron/gamma pulse shape discrimination, Nucl. Instrum. Meth. A, 266 (2012) 88-93.
[6] E.V.v. Loef, Plastic scintillators with neutron-gamma pulse shape discrimination, IEEE Trans. Nucl. Sci., 61 (2014) 467-471.
[7] P.N. Zhmurin, V.N. Lebedev, A.F. Adadurov, V.N. Pereymak, Y.A. Gurkalenko, Pulse shape neutrons and gamma quanta discrimination by means of plastic scintillator of the new generation, Funct. Mater., 20 (2013) 500-503.
[8] N.P. Hawkes, G.C. Taylor, Analysis of the pulse shape mechanism in a plastic scintillator with efficient neutron/gamma pulse shape discrimination, Nucl. Instrum. Meth. A, 729 (2013) 522-526.
[9] H.P. Martinez, I. Pawełczak, A.M. Glenn, M.L. Carman, N. Zaitseva, S. Payne, Pulse shape discrimination in nonaromatic plastics, Nucl. Instrum. Meth. A, 771 (2015) 28-31.
[10] S.A. Pozzi, M.M. Bourne, S.D. Clarke, Pulse shape discrimination in the plastic scintillator EJ-299-33, Nucl. Instrum. Meth. A, 723 (2013) 19-23.
[11] D. Cester, G. Nebbia, L. Stevanato, F. Pino, G. Viesti, Experimental tests of the new plastic scintillator with pulse shape discrimination capabilities EJ-299-33, Nucl. Instrum. Meth. A, 735 (2014) 202-206.

[12] P.N. Zhmurin, V.N. Lebedev, V.D. Titskaya, A.F. Adadurov, D.A. Elyseev, V.N. Pereymak, Polystyrene-based scintillator with pulse-shape discrimination capability, Nucl. Instrum. Meth. A, 761 (2014) 92-98.
[13] G.H.V. Bertrand, M. Hamel, S. Normand, Pulse shape discrimination between (fast or thermal) neutrons and gamma-rays with plastic scintillators: State of the art, Nucl. Instrum. Meth. A, In Press (2014).
[14] I.A. Pawełczak, A.M. Glenn, H.P. Martinez, M.L. Carman, N.P. Zaitseva, S.A. Payne, Boron-loaded plastic scintillator with neutron-γ pulse shape discrimination capability, Nucl. Instrum. Meth. A, 751 (2014) 62-69.
[15] N. Zaitseva, A. Glenn, H.P. Martinez, L. Carman, I. Pawełczak, M. Faust, S. Payne, Pulse shape discrimination with lithium-containing organic scintillators, Nucl. Instrum. Meth. A, 729 (2013) 747-754.
[16] I.G. Britvich, V.G. Vasil'chenko, V.N. Kirichenko, S.I. Kuptsov, V.G. Lapshin, A.P. Soldatov, A.S. Solov'ev, V.I. Rykalin, S.K. Chernichenko, I.V. Shein, New polystyrene-based scintillators, Instrum. Exp. Tech. +, Translated from Prib. Tekh. Eksp., 45 (2002) 644-654.
[17] N.J. Cherepy, R.D. Sanner, P.R. Beck, E.L. Swanberg, T.M. Tillotson, S.A. Payne, C.R. Hurlbut, Bismuth- and lithium-loaded plastic scintillators for gamma and neutron detection, Nucl. Instrum. Meth. A, 778 (2015) 126-132.
[18] L.R. Greenwood, N.R. Chellew, G.A. Zarwell, 6Li-loaded liquid scintillators with pulse-shape discrimination, Rev. Sci. Instrum., 50 (1979) 472-477.
[19] H.H. Ross, R.E. Yerick, A new liquid scintillator for thermal neutron detection, Nucl. Sci. Eng., 20 (1964) 23-27.
[20] I. Sen, D. Penumadu, M. Williamson, L.F. Miller, A.D. Green, A.N. Mabe, Thermal neutron scintillation detectors based on poly(2-vinylnaphthalene) composite films, IEEE Trans. Nucl. Sci., 58 (2011) 1386-1393.
[21] N. Zaitseva, J. Newby, G. Hall, C. Saw, L. Carman, N. Cherepy, S. Payne, Growth and properties of lithium salicylate single crystals, Cryst. Growth Des., 9 (2009) 3799-3802.
[22] U. Olsher, Coordination chemistry of lithium ion: A crystal and molecular structure review, Chem. Rev., 91 (1991) 137-164.